

# MODELING OF MAGNETORHEOLOGICAL MOUNTS IN VARIOUS OPERATION MODES

Janusz GOŁDASZ\*, Bogdan SAPIŃSKI\*\*

\* Technical Center Kraków, BWI Group Poland, ul. Podgórk Tynieckie 2, 30-399 Kraków, Poland

\*\* Department of Process Control, AGH University of Science and Technology, al. Mickiewicza 30, 30-059 Kraków, Poland

[janusz.goldasz@bwigroup.com](mailto:janusz.goldasz@bwigroup.com), [deep@agh.edu.pl](mailto:deep@agh.edu.pl)

**Abstract:** Recent advances in the research of magnetorheological/electrorheological (MR/ER) fluid based devices have indicated the opportunities for smart fluid based devices utilizing more than one operation mode. As such, the purpose of the present research is to draw attention to the existing models of magnetorheological (MR) mounts operating in two of the three fundamental operating modes, namely, the flow mode and the squeeze mode, and to highlight the potential applications of these modes in hydraulic mount applications. Therefore, in the paper the authors focus on recent applications of MR/ER fluids in that domain, and then proceed to summarizing the modeling principles for the two operation modes followed by a finite-element magnetostatic analysis of the mount's magnetic circuit, parameter sensitivity study and exemplary numerical simulations of each mode. The simulation results are converted into the frequency domain and presented in the form of dynamic stiffness and damping vs. frequency plots, respectively.

## 1. INTRODUCTION

Nearly all magnetorheological/electrorheological (MR/ER) devices can be classified as operating in at least one of the following three operation modes: flow mode, shear mode, and squeeze mode as shown in in Fig. 1. The devices operating in either flow mode or shear mode (linear/rotary shock absorbers, clutches, engine mounts) have been commercialized, and the theory well developed (Philips, 1969; Gavin et al., 1996a; Gavin et al., 1996b; Wiliams et al., 1993, Sproston et al., 1994).

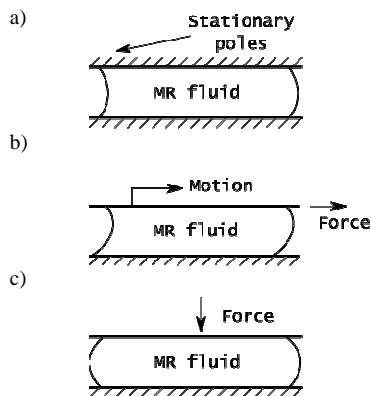


Fig. 1. Configurations of MR hardware: a) flow mode, b) shear mode, c) squeeze mode (Jolly et al., 1998)

For example, BWI Group (formerly the Chassis Division of Delphi Corp.) has developed and implemented an MR flow-mode based shock absorber (Hopkins et al., 2001; Kruckemeyer et al., 2001) (known under the commercial name of MagneRide) and an MR flow-mode based powertrain mount for the automotive industry (Baudendistel et al., 2002, Baudendistel et al., 2003). Also, Lord Corp.

has been rather active in developing commercial applications of flow-mode MR dampers as well as shear-mode rotary MR dampers (brakes) (Carlson et al., 1994; Jolly, 1998). To the authors' best knowledge, no commercial applications of the squeeze-mode based hardware have been reported. There is, however, an ongoing engineering and research interest in the development of MR/ER fluid based hardware operating in the squeeze-mode (Wiliams et al., 1993; Sproston et al., 1994; Jolly and Carlson, 1996, Bolter and Janocha, 1998; Tang et al., 1998, Stanway et al., 2000, Farjoud et al., 2009). In the case of MR fluid, the devices employ a layer of MR fluid sandwiched between two magnetic poles of which at least one is subjected to vertical motion. As a result, the distance between the poles varies according to the displacement or force profile, and the fluid is forced out of the between them. The squeeze-mode seems very suitable for low-stroke (few millimeters or less) and high damping force MR/ER applications, namely powertrain mounts or general-purpose vibration isolators. As such, controllable squeeze-mode devices can be more compact when sized for same damping force requirements. Research challenges are due to the squeeze-mode model capable of predicting flow field, pressure distribution across squeezing plates and shear stresses (Farjoud et al., 2011), control schemes (Zhang et al., 2011). Manufacturing challenges may arise, though, due to the range of displacements required for effective operation.

However, ER fluids may not be suitable for implementing a real-world squeeze-mode device as one of the failure modes of such hardware is due to the contact of squeezing plates (and electrical short circuit). MR fluid squeeze-mode applications may be less problematic in that regard.

At the present moment, the most novel and promising squeeze-mode application seems a mixed-mode MR fluid-based damper or an MR mount (Brigley et al., 2007, Minh, 2009). Such a device might utilize the flow mode for large stroke motion damping, and make use of the squeeze flow

mode in order to enhance the primary flow mode in controlling small amplitude displacements. So far, several research studies have been conducted in that regard and a rather thorough summary of the recent research efforts was described by Minh (2009).

Therefore, the purpose of the research is to draw attention to the existing models of MR mounts operating in two of the above mentioned modes (flow, squeeze), and to highlight the potential applications of these modes in hydraulic mount applications (e.g. automotive powertrain mounts).

As such, the authors highlight some applications of MR/ER fluids in that domain, and then proceed to summarizing the modeling principles for the two operation modes followed by a finite-element magneto-static analysis of the mount's magnetic circuit, a parametric study and exemplary simulations of each mode.

## 2. MR HYDRAULIC MOUNT

The flow-mode MR damper is the smart-fluid based device that has been most commercialized over the years in a number of automotive vehicle platforms in particular (Alexandridis, 2007). The number of reported automotive MR damper applications well exceeds twenty in Europe, Asia, and US. Recent application areas also include military vehicle suspension applications (Lord Corp.). By a wide margin, it is the MR damper of the conventional deCarbon monotube design that is the most often implemented MR fluid based device. Apparently, another MR device under development is the MR hydraulic mount for powertrain applications (Baudendistel et al., 2002). The MR mount is claimed to operate in flow mode. Most ER fluid based mounts or MR fluid based ones follow the same design principle that conventional passive mounts are based upon, and with smart fluids the mount stiffness and damping characteristics can be controlled in real-time.

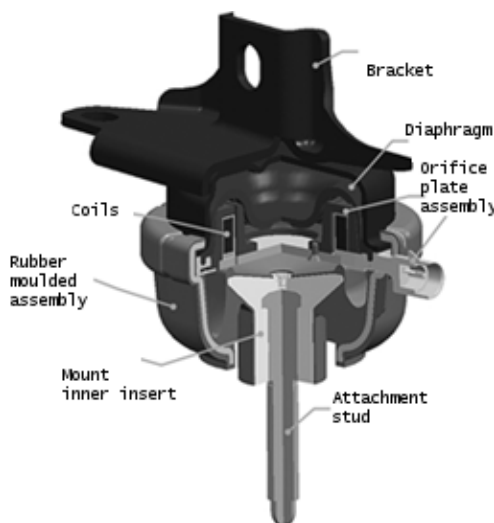


Fig. 2. MR hydraulic mount (courtesy of BWI Group)

As shown in Fig. 2, the components of each mount are rubber shells each constituting a fluid chamber filled with smart fluid and incorporating flow paths for the fluid.

The upper volume is the pumping chamber, and the lower one is the so-called reservoir. In the case of MR mounts, the flow path is designed in such a way to be enveloped by the magnetic field generated in the circuit. With MR mounts, the presence of the magnetic field causes the smart fluid's yield stress to be altered according to the level of the magnetic field strength across the flow path height. As described by Baudendistel et al. (2002, 2003) two optional components of the MR mount are the so-called inertia track, and the decoupler. The decoupler is usually a partitioning plate located in a bypass flow path. With passive mounts it is a feature for providing means for enhancing the mount in isolating the low-displacement, high-frequency inputs, whereas the inertia track (in the form of a long de-energized fluid channel) is used as an additional feature for controlling the fluid flow at low frequencies (Singh et al., 1992). These features have been widely used in passive conventional hydraulic mounts; however, their applications in MR mounts are none.

Active or semi-active mounts for have been of great interest for the automotive industry OEMs (Original Equipment Manufacturers) (Kowalczyk et al., 2004). Those mounts are capable of overcoming the conflicting design requirements of standard passive hydraulic mounts to deliver a device that is capable of providing a stiff support for the engine and good isolation at the same time.

## 3. MODELING OF MR MOUNTS

The following sections contain a brief summary of MR mount displacement-driven models operating in flow mode, squeeze mode, and the mixed mode (combined flow mode and squeeze mode), respectively.

### 3.1. Flow mode

The flow mode MR hydraulic mount exemplary configuration is shown in Fig. 3. The annular gap is contained in the stationary core. The magnetic field strength  $H$  is perpendicular to the surfaces of the annulus in the piston in order to restrict the fluid motion in the direction perpendicular to the surfaces of the annulus. A majority of the magnetic field strength  $H$  is generated in the circuit incorporating the core, the fluid volume contained in the annulus, and the outer ring of the core. The height of the annular gap is  $h$ ,  $b$  is the mean radius of the annulus, and the cross-sectional area of the annular gap is  $A_g = bh$ . Also, the upper chamber cross-sectional area is  $A_p$ . The combined length of the active pole sections is  $L_a$  (the total length of the annular gap is  $L_g$ ). The MR fluid is characterized by the bulk modulus  $\beta$ , the density  $\rho$ , the field-induced yield stress  $\tau_0$ , and the field-invariant base viscosity  $\mu$ . The top of the mount is driven by the known external displacement profile  $x(t)$  (or the velocity  $v(t)$ ), and the motion of the upper member forces the fluid to flow from one chamber to the other. The pressure drop across the stationary core is  $\Delta P = P_1 - P_2$ , where  $P_1$  and  $P_2$  are pressures in the fluid chambers above and below the core assembly, respectively. The compliance of the upper chamber is  $C_1$ , and that of the lower one is  $C_2$ .

The volume flow rate through the annulus is  $Q$ . The geometry of the mount may contain a bypass path characterized by the hydraulic diameter  $H_b$  (the discharge coefficient  $C_b$  and the area  $A_b$ ). The volume flow rate through the bypass is  $Q_b$ .

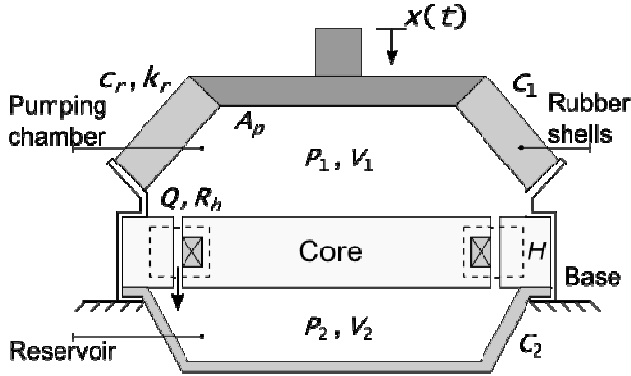


Fig. 3. Flow mode MR mount (Baudendistel et al., 2002); dashed lines show the magnetic field strength lines  $H$

To arrive at the equations governing the behavior of the mount, the volumetric approach is used to describe pressure variations in each chamber. The method has been used in analyzing passive shock absorbers (Lee, 1997) and is common in engine mount analyses (Adiguna et al., 2003). Also, an inertia track model is implemented into the mount's model to account for the lumped mass of fluid in the annulus inertia (Singh et al., 1992, Kim and Singh, 1993, He and Singh, 2007). The hydraulic losses at the entry to the annulus (and the exit of the annular gap) and the effects of fluid flow development in the annulus are omitted, too. Then, the following set of equations can be drawn:

$$\begin{aligned} \frac{dP_1}{dt} &= \frac{A_p v - (Q + Q_b)}{C_1} \\ \frac{dP_2}{dt} &= \frac{Q + Q_b}{C_2} \\ \frac{dQ}{dt} &= \frac{A_g}{\rho L_g} (P_1 - P_2 - \Delta P_{MR}) \end{aligned} \quad (1)$$

Briefly, Eq. 1 accounts for the pressure variations in each fluid chamber and the fluid mass inertia when bouncing on compliant fluid volumes. The pressure drop  $\Delta P_{MR}$  across the annulus can be expressed as given by Gavin et al. (1996a, 1996b):

$$\Delta P_{MR} \approx 8 \frac{\mu Q L_a}{bh^3} (1 + 3T) \left[ \cos \left( \frac{1}{3} a \cos \left( 1 - 54 \left( \frac{T}{1 + 3T} \right)^3 \right) \right) + \frac{1}{2} \right] \quad (2)$$

where  $T$  is the non-dimensional yield stress:

$$T = \frac{bh^2 \tau_0}{12\mu Q} \quad (3)$$

Eq. 2 utilizes the solution of the Bingham model governing the quasi-steady-state relationship between the flow rate through the energized gap and the field-induced pressure drop in flow mode (Philips, 1969). The bypass flow rate  $Q_b$  is as follows:

$$Q_b = C_b A_b \sqrt{2 \frac{|P_1 - P_2|}{\rho}} \text{sign}(P_1 - P_2) \quad (4)$$

In the absence of magnetic field the laminar flow in the flow path is assumed. Therefore, the pressure drop at the de-energized (OFF) condition is:

$$\Delta P_{MR} = 12 \frac{\mu L_g}{bh^3} Q \quad (5)$$

Moreover, assuming the mass  $M$  is attached to the upper base the equation governing the mass inertia can be derived as follows:

$$M \frac{dv}{dt} + c_r v + k_r x = A_p P_1 \quad (6)$$

where  $c_r$  and  $k_r$  are the rubber damping coefficient and the stiffness ratio, respectively. The equations represent a set of expressions governing the force of flow mode MR mounts.

### 3.2. Squeeze mode

The squeeze mode MR mount is shown in Fig. 4. In this configuration the lower pole is stationary, whereas the upper pole is driven by the displacement  $x(t)$ . Also, a planar plate is attached to the upper fixture. The initial gap across the upper plate and the upper surface of the core is  $h_0$ .

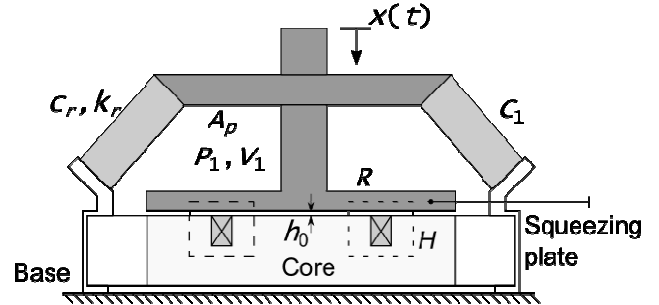


Fig. 4. Squeeze mode MR mount (Gołdasz and Sapiński, 2011); the magnetic field strength  $H$  shown with dashed lines

Then, the continuity equations and the MR squeeze mode expressions can be derived in the following manner (Kim et al., 1998, Stanway et al., 2000, Hong et al., 2002; Farjoud et al., 2009):

$$\begin{cases} \frac{dP_1}{dt} = \frac{A_p v}{C_1} \\ c_{sq} = \frac{3\mu\pi R^3}{2(h_0 + x)^3} \\ F_{sq} = \tau_0 \frac{3\pi R^3}{4(h_0 + x)} \text{sgn}(v) \end{cases} \quad (7)$$

Finally, the mass inertia can be described as follows:

$$M \frac{dv}{dt} + c_r v + c_{sq} v + F_{sq} + k_r x = A_p P_1 \quad (8)$$

where  $c_{sq}$  is the viscous damping coefficient in the absence of magnetic field,  $F_{sq}$  is the field induced force, and  $R$  is the outer radius of the upper plate. The first of the equa-

tions in the above set accounts for the compliance effects of the MR squeeze mode mount (chamber compliance). The above equations represent a set of expressions governing the output of squeeze mode MR mounts.

### 3.3. Mixed mode

The mixed mode mount shown in Fig. 5 include the pumping chamber, the reservoir chamber, and the stationary core incl. the annular gap. The magnetic field that is induced in the gap (upon the application of current in the primary coil) is perpendicular to the fluid flow (flow mode). The other coil faces the plate opposing the upper surface of the core.

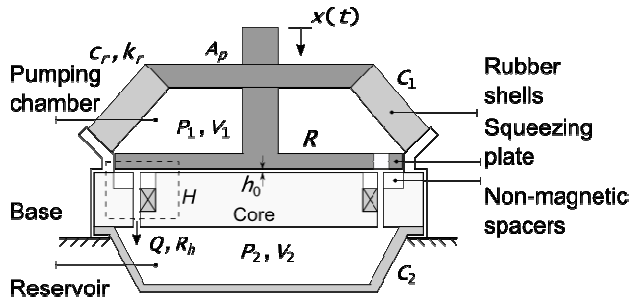


Fig. 5. Mixed-mode MR mount (Minh, 2009)

As a result of the plate displacement squeezing occurs. Both circuits can operate independently or in series. In this layout the flow-mode MR mount equations can be modified to include the squeeze mode circuit as follows (Minh, 2009):

$$\frac{dP_1}{dt} = \frac{A_p v - (Q + Q_b)}{C_1} \quad (9)$$

$$\frac{dP_2}{dt} = \frac{Q + Q_b}{C_2}$$

$$\frac{dQ}{dt} = \frac{A_g}{\rho L_g} (P_1 - P_2 - \Delta P_{MR})$$

$$M \frac{dv}{dt} + (c_r + c_{sq})v + F_{sq} + k_r x = A_p P_1 \quad (10)$$

where  $\Delta P_{MR}$  is the field induced pressure drop defined In Section 3.1. Again, entry/exit effect are omitted in the analysis. Eqs. 9 and 10 reveal a set of expressions governing the dynamic output of mixed mode MR mounts. The equations may present a squeeze mode MR mount, a flow mode mount or a mixed mode mount. For instance, freezing the flow in the annulus by setting the yield stress In the flow path to a high level results in no-flow conditions and reduces the set of Eqs. 9 and 10 to the system of Eqs. 7 and 8. Also, setting the large initial gap between the squeezing plate and the core removes the squeeze mode contribution, and the flow mode can be studied on its own.

## 4. NUMERICAL SIMULATIONS

The numerical simulations include the development of a two-dimensional axi-symmetric model of the mixed

mode MR mount of Fig. 5, the parameter sensitivity study as well as calculations of the complex transfer function of the MR mount when subjected to a sweep-sine constant amplitude displacement input.

The geometry and material properties of a mixed-mode mount virtual prototype are shown in Table 1. The data contained in the table represent the base configuration of the MR mount virtual prototype.

Tab. 1. Geometry and material properties of the MR mount

Symbol	Description	Value
$A_p, \text{mm}^2$	Mount effective area	2827
$C_1, \text{N/mm}^5$	Pumping chamber compliance	3100
$C_2, \text{N/mm}^5$	Reservoir chamber compliance	120000
$L_g, \text{mm}$	Annulus length	31
$L_{a_s}, \text{mm}$	Active length (flow mode)	13
$h_1, \text{mm}$	Annulus height (gap)	1.8
$A_g, \text{mm}^2$	Annulus cross-section area	281.6
$R, \text{mm}$	Plate radius (squeeze mode)	21
$h_0, \text{mm}$	Initial gap (squeeze mode)	{1, 3}
$H_b, \text{mm}$	Bypass size	0
$\rho, \text{g/cm}^3$	MR fluid density	3.1
$\mu, \text{Ns/mm}^2$	MR fluid viscosity	0.00000003
$k_r, \text{N/mm}$	Rubber stiffness	200
$c_r, \text{Ns/mm}$	Rubber damping	0.1

### 4.1. Magnetostatic model

Two-dimensional axi-symmetric simulations (using the finite-element platform FEMM) were needed to optimize the geometry of the mount and to extract the flux density data for each gap that are necessary calculating the yield stress levels. Both coils were assumed to take on currents up to 500 ampere turns (AT). The  $B-H$  curve for the MR fluid is shown in Fig. 6 and SAE 1010 material properties were assumed for components in the magnetic circuit. The exemplary distributions of the magnetic field in the circuits at 500 ampere turns each are shown in Figs. 7 through 9.

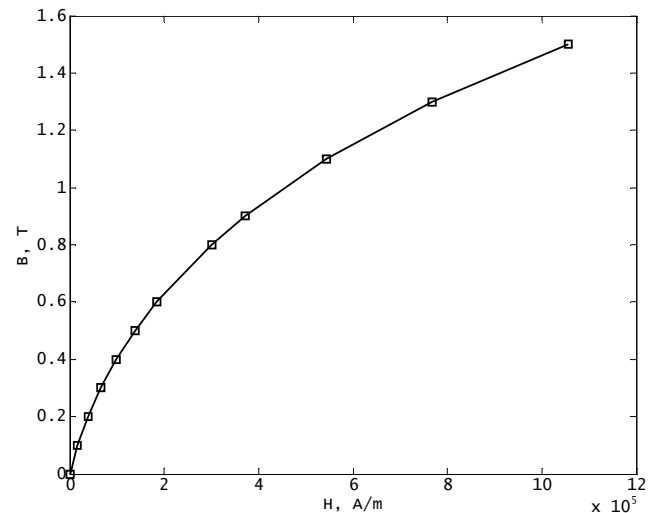


Fig. 6. MR fluid  $B-H$  curve (courtesy of BWI Group)

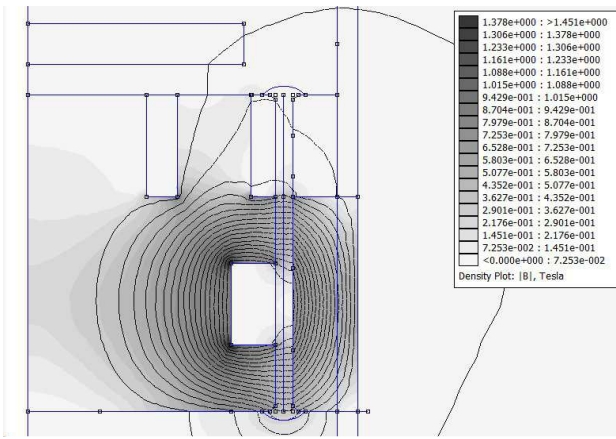


Fig. 7. Primary (flow-mode) coil; 500 AT

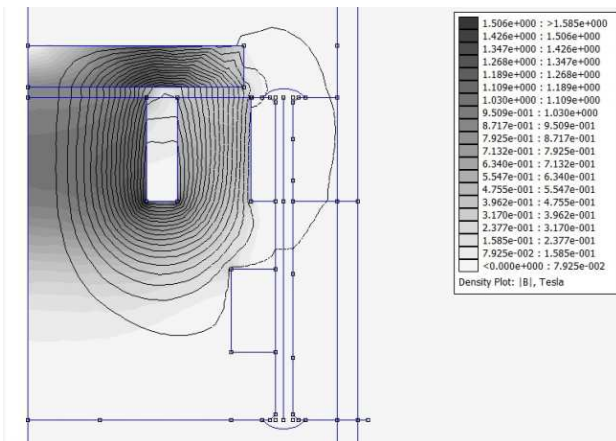


Fig. 8. Secondary (squeeze-mode) coil; -500 AT,  $h_0=1.0$  mm

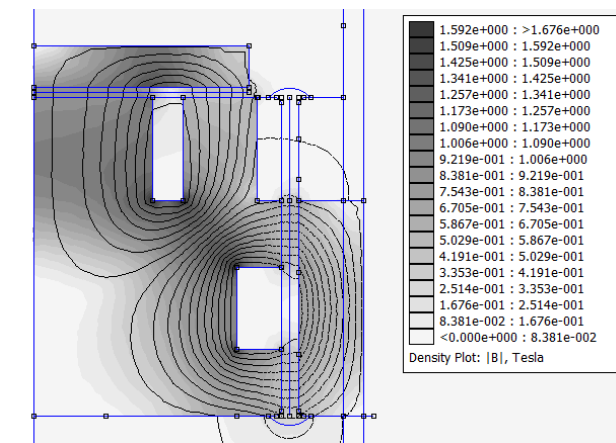


Fig. 9. Primary coil and secondary coil at ON condition

It is apparent from the illustrations both circuits can be operated independently with little influence of one mode on the other. For example, raising the coil current in the squeeze mode circuit even up to 500 ampere turns has little effect on the magnetic field strength in the switched off flow-mode annulus, and the calculated flux density level is less than 0.04 T.

The averaged flux density distribution (normal component) in the radial direction for the squeeze mode circuit AT the initial distance of 1.0 mm is revealed in Fig. 10, and the flux density vs. ampere turns vs. plate-to-core distance mapping is illustrated in Fig. 11. As shown in the

images, the flux density in the squeeze mode gap is rather uniform; however, there is a significant difference in the flux density level across the inner and outer pole area, respectively. The results indicate there is some need for improvement and further optimization required in the squeeze mode circuit geometry.

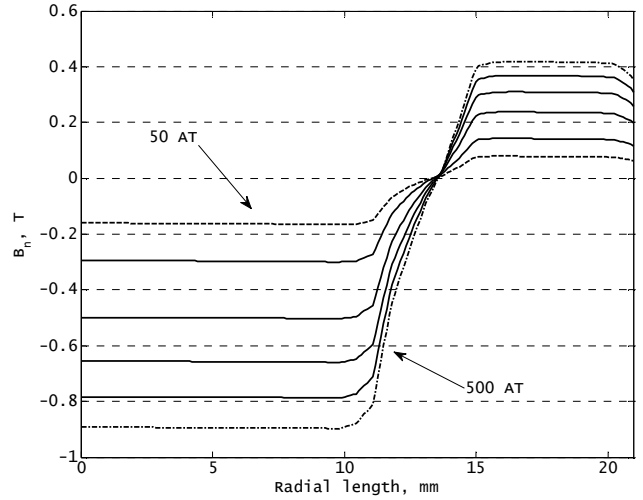


Fig. 10. Flux density distribution, squeeze mode;  $h_0=1.0$  mm

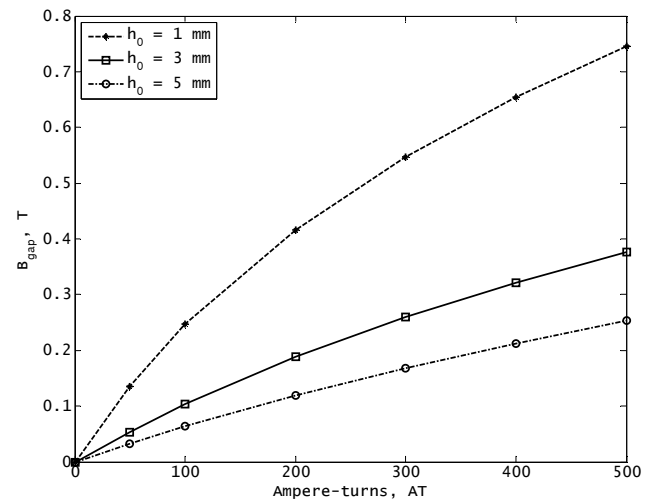


Fig. 11. Averaged flux density in the annulus, squeeze mode

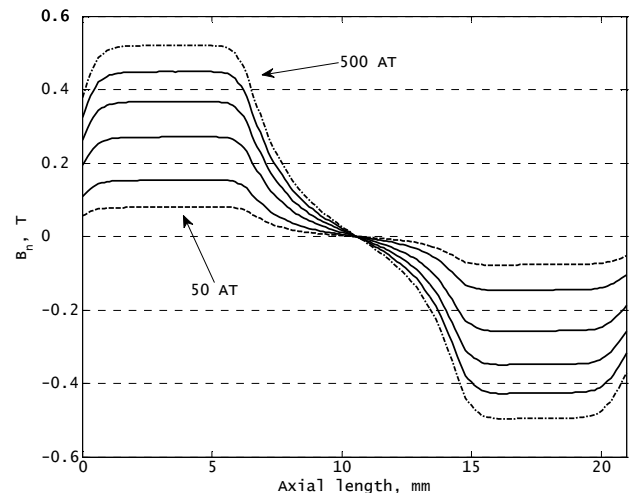


Fig. 12. Flux density distribution, flow mode

Similarly, the distribution of the averaged flux density normal component along the annulus (in the axial direction) and the flux density vs. ampere turns mapping for the flow mode circuit are shown in Figs. 12 and 13, respectively. The flux density distribution in the annulus is almost symmetrical across the two poles with little flux leakage to the other circuit.

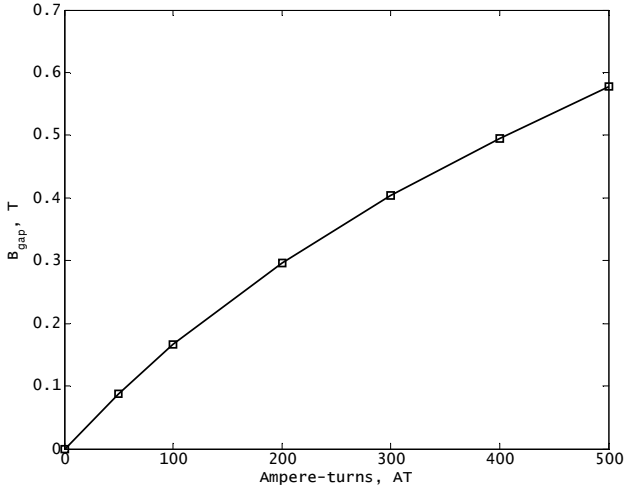


Fig. 13. Averaged flux density in the annulus, flow mode

#### 4.2. Parameter sensitivity study

The parameter sensitivity study was required to understand the effect of material properties and geometric variables on the performance of the MR mount. To accomplish this, the mount model (at OFF condition) in Simulink was subjected to a sweep-sine constant amplitude displacement input. The results in time domain were the transmitted force and the input displacement. In all tests the input displacement amplitude was 2 mm, and the frequency varied from 0 to 300 Hz. The data were then converted into the frequency domain using FFT with Matlab – see Figs. 14–25. The MR mount performance metric of interest in the frequency domain is the so-called dynamic stiffness  $K_{dyn}$ . By definition, the dynamic stiffness is the ratio of the force to the displacement in frequency domain of the following form (Kim et al., 1993):

$$K_{dyn}(\omega) = \frac{F(\omega)}{X(\omega)} \quad (11)$$

where  $F(\omega)$  and  $X(\omega)$  are the frequency domain force and stroke, respectively. It is a complex variable from which the amplitude  $|K_{dyn}|$  and phase  $\phi$  can be calculated. Calculating the damping effects requires the calculation of the so-called dynamic damping  $C_{damp}$  in the following form:

$$C_{damp}(\omega) = \frac{K_{dyn}(\omega) \cdot \sin(\omega)}{\omega} \quad (12)$$

Both metrics are common when analyzing dynamic system data and have been used in the present study. At the OFF condition the contribution of squeeze mode is small, therefore, the study focused on the flow mode geometry and the material properties at this point. The parametric

study involved the following flow mode parameters: annulus length  $L_g$ , gap size  $h$ , bypass size  $H_b$ , pumping chamber compliance  $C_1$ , base viscosity  $\mu$ , and density  $\rho$ .

The influence of the annulus length  $L_g$  is shown in Figs. 14 and 15. Here, increasing the annulus length decreases the fluid resonant frequency. This effect is due to the larger mass of the fluid contained in the annulus.

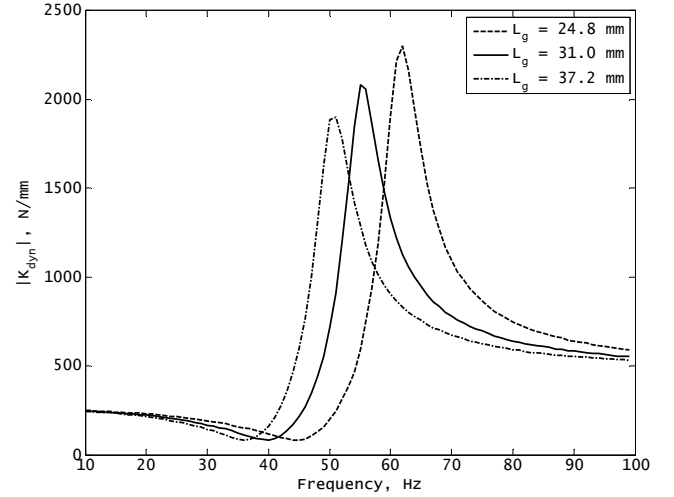


Fig. 14. Dynamic stiffness: influence of gap length,  $L_g$

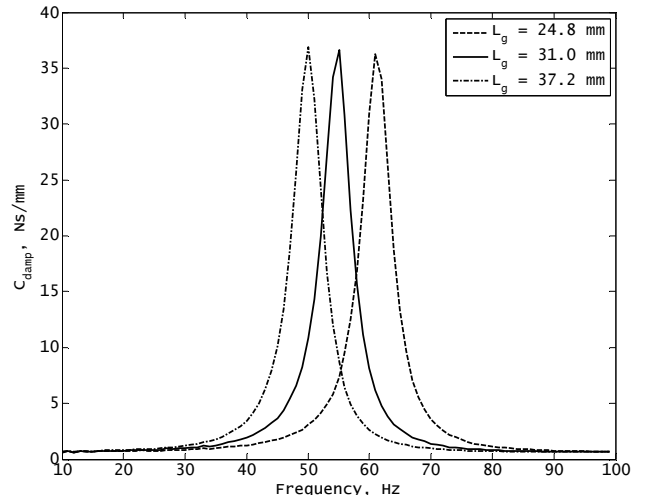


Fig. 15. Damping: influence of annular gap length,  $L_g$

For comparison, increasing the gap size results in higher resonance frequencies of the fluid – see Figs. 16 and 17. Also, increasing the stiffness of the upper chamber (and decreasing the compliance  $C_1$ ) shifts the resonant frequency towards higher frequencies as seen in Figs. 18 and 19. In addition to that, the respective effects of the bypass size and the viscosity lower the amplitude of the resonant frequency peaks as seen in Figs. 20 through 23. Also, increasing the density of the fluid results in an effect that is similar to the influence of the annulus length – see Figs. 24 and 25. It is due to the increased mass of the fluid in the annulus.

Also, it is interesting to note the reduction in the amplitude of the notch frequency (located below the fluid resonance) was achieved through varying the bypass flow path geometry, and changing the viscosity of the MR fluid.

Other parameters resulted in varying the location of the notch frequency (along with the resonance frequency) but not the amplitude.

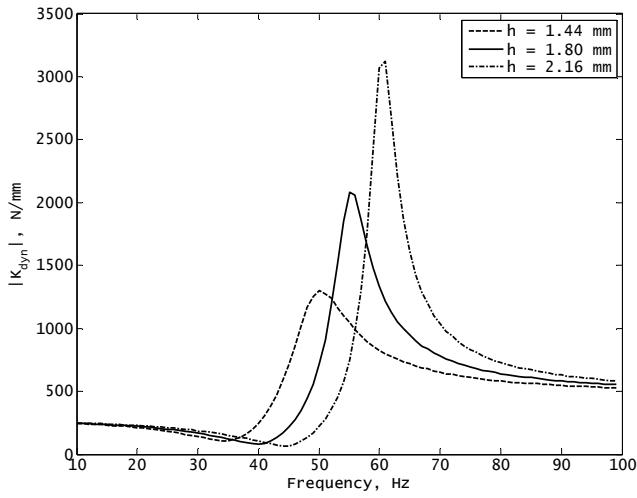


Fig. 16. Dynamic stiffness: influence of annular gap size,  $h$

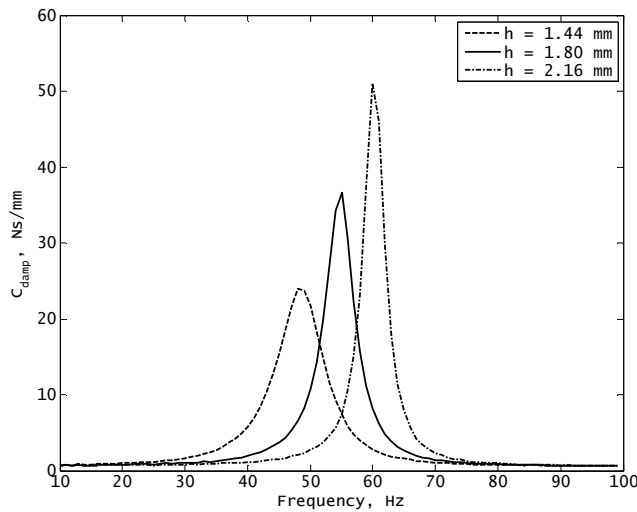


Fig. 17. Damping: influence of annular gap size,  $h$

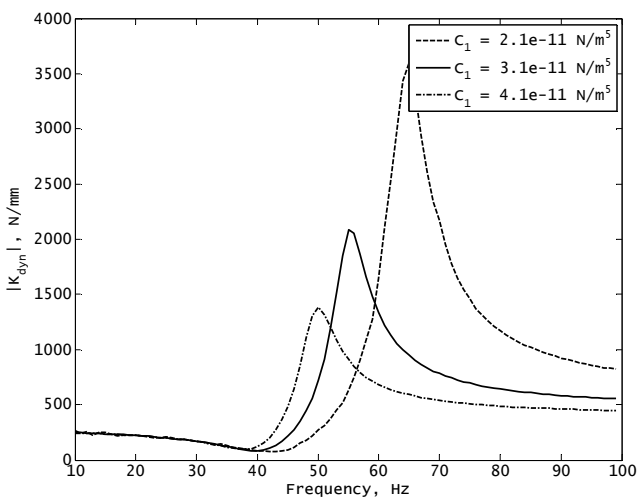


Fig. 18. Dynamic stiffness: pumping chamber compliance,  $C_1$

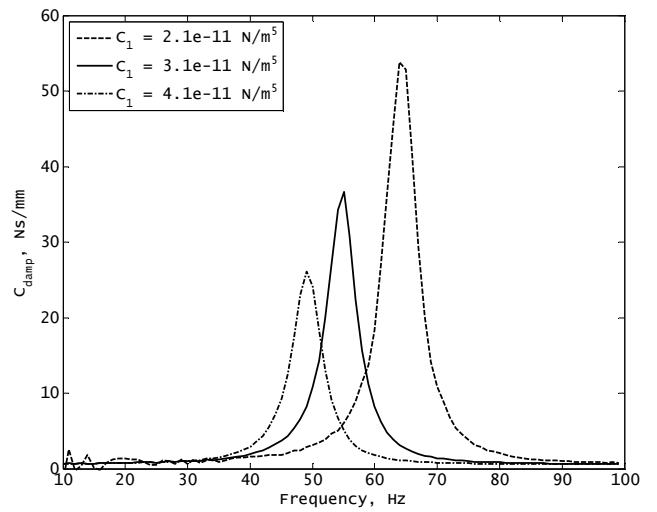


Fig. 19. Damping: pumping chamber compliance,  $C_1$

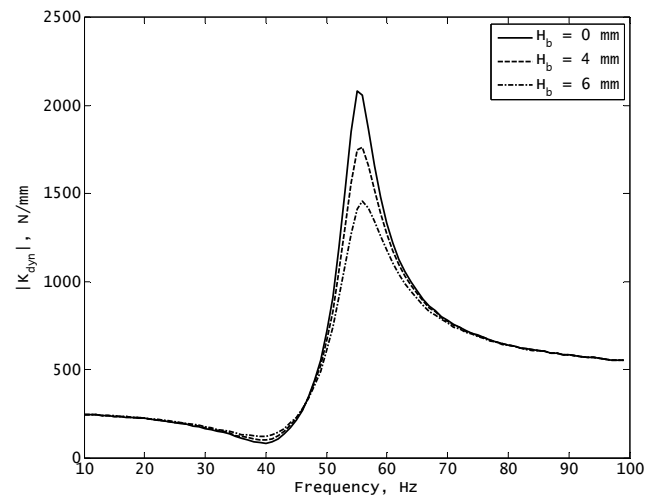


Fig. 20. Dynamic stiffness: influence of bypass path size,  $H_b$

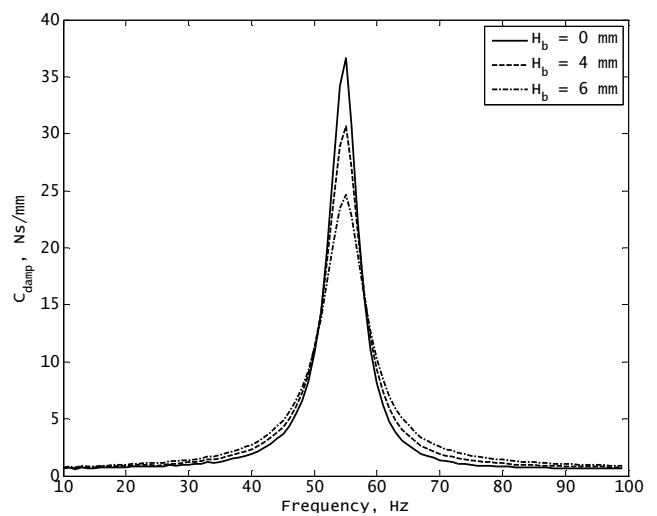
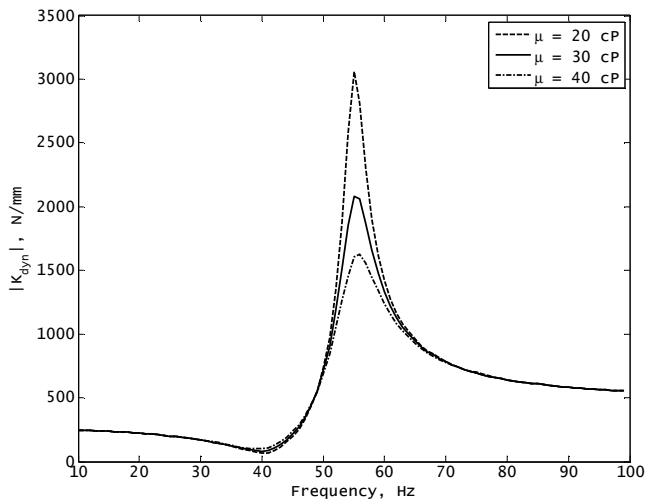
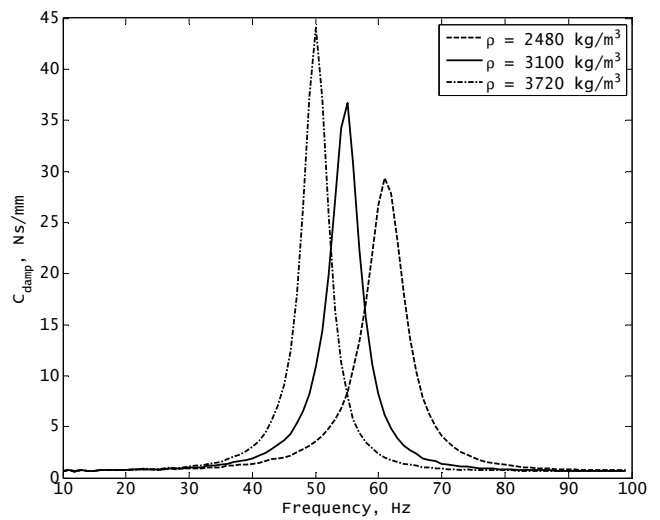


Fig. 21. Damping: influence of bypass path size,  $H_b$



**Fig. 22.** Dynamic stiffness: influence of fluid base viscosity,  $\mu$



**Fig. 25.** Damping: influence of fluid density,  $\rho$

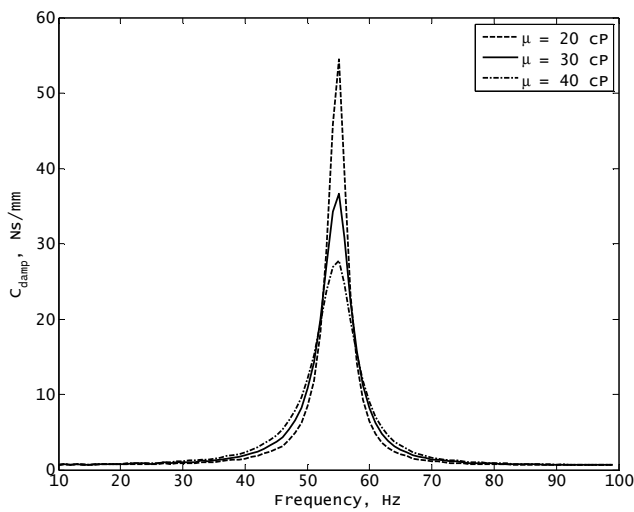


**Fig. 23.** Damping: influence of fluid base viscosity,  $\mu$

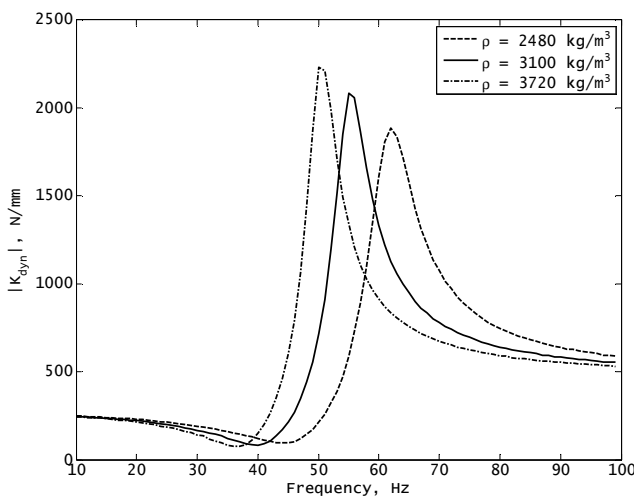


**Fig. 24.** Dynamic stiffness: influence of fluid density,  $\rho$

### 4.3. Effect of magnetic field

The effect of magnetic field on the MR mount characteristics is illustrated in Figs. 26–33. Again, the data were obtained by running sweep-sine numerical tests on the mount model described by Eqs. 9 and 10. Each mode was first investigated on its own without the contribution of the other mode. For example, the flow mode tests were configured to minimize the contribution of the squeezing plate. As such, the initial gap between the core surface and the squeezing plate  $h_0$  was set to 3 mm, and the stroking amplitude to 2 mm. Also, the squeeze mode coil was powered OFF. Then, the contribution from the viscous force in the squeeze mode gap is almost none, and squeezing of fluid does not interfere with flow mode. The results are shown in Figs. 26 and 27.

For comparison, the squeeze mode tests first involved cutting off the MR fluid flow in the annulus by setting the coil current level to a large value (above 200 ampere turns), and powering the squeeze mode coil circuit. As already mentioned, at this condition the MR mount model reduces to the configuration described in Section 3.2. Moreover, in order to observe the contribution of the squeeze mode on the flow mode performance the flow mode circuit was set to the OFF condition, and the squeeze mode coil current varied from 0 to 500 ampere turns. Also, the initial distance between the squeezing plate and the core surface was set down to 1 mm, and the stroking amplitude to 0.7 mm. The results are revealed in Figs. 28 and 29 (frozen annulus) as well as 30 and 31. At this condition, the pressure drop across the annulus is less than the field-induced yield stress, and the fluid flow is effectively eliminated so that there is no contribution of the fluid in the annulus to the damping, and the performance characteristics of the mount are solely controlled by the squeeze mode circuit and the mount rubber stiffness and damping, respectively.

The squeeze mode contribution modifies the stiffness (and the damping) rather uniformly across the frequency range. The squeeze mode effect is additive, and does not interact with the flow-mode directly. It is consistent with observations of other researchers (Minh, 2009). The effect

is related to the addition of a parallel spring (and a dashpot) of variable stiffness (and damping).

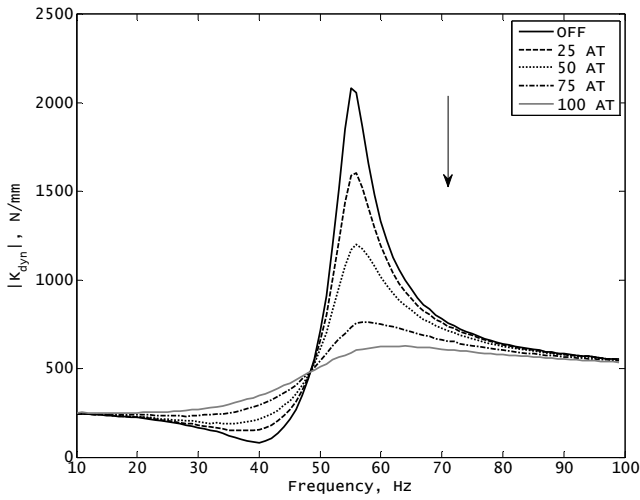


Fig. 26. Dynamic stiffness: magnetic field change; flow mode

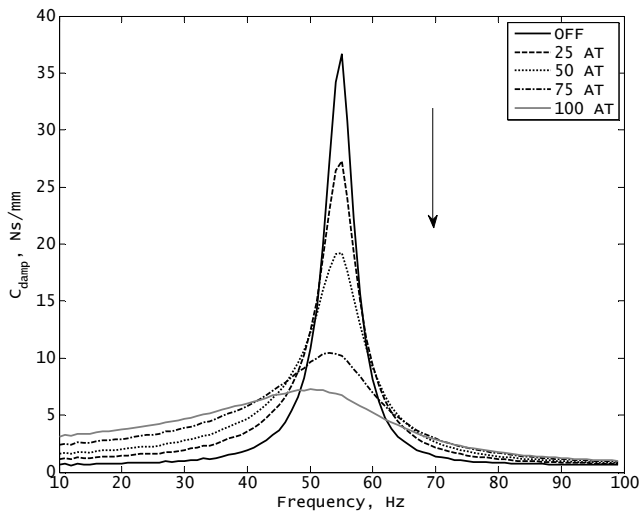


Fig. 27. Damping: magnetic field change; flow mode

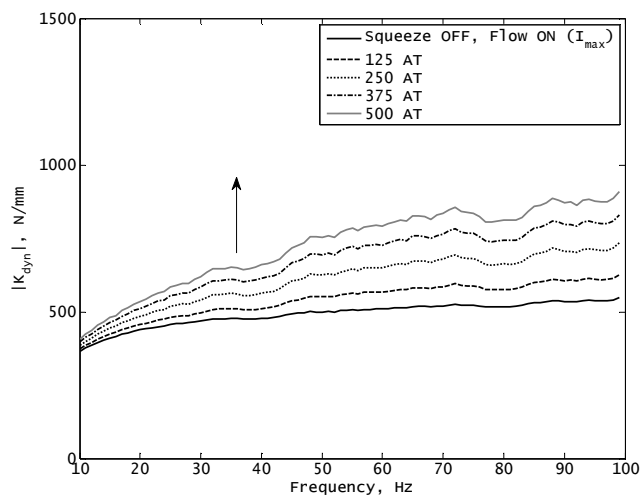


Fig. 28. Dynamic stiffness: magnetic field; squeeze mode

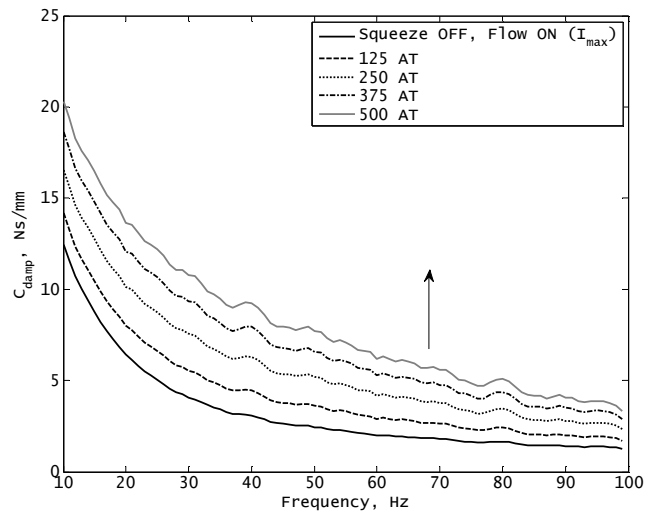


Fig. 29. Damping: influence of magnetic field; squeeze mode

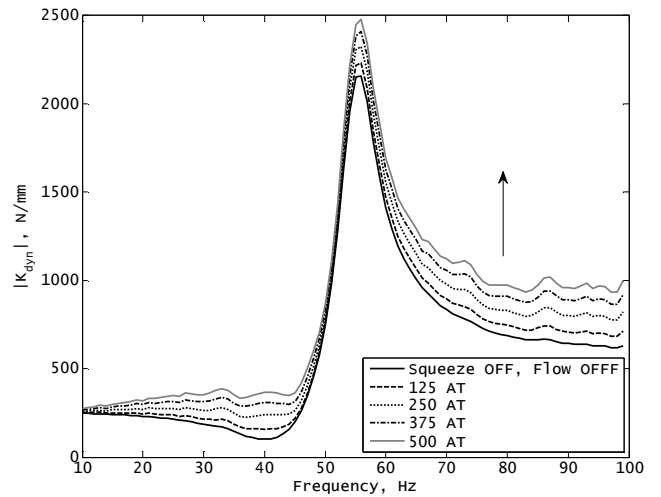


Fig. 30. Dynamic stiffness: magnetic field; squeeze mode

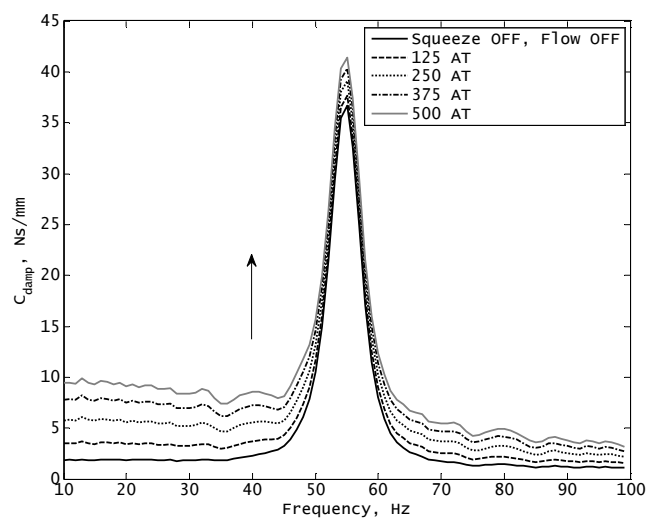


Fig. 31. Damping: squeeze mode (flow mode at OFF condition)

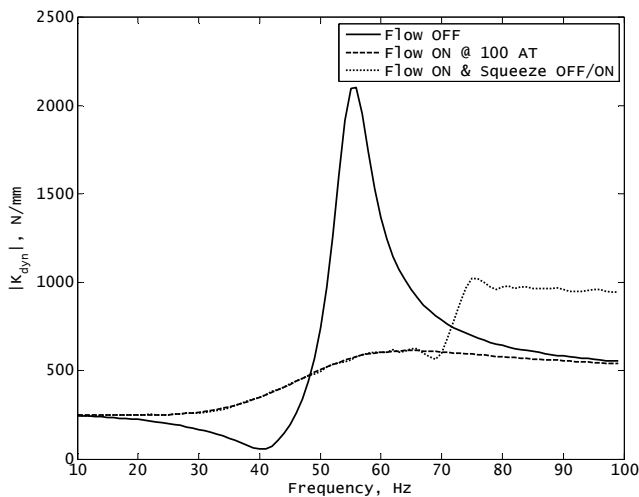


Fig. 32. Dynamic stiffness: simple control scheme

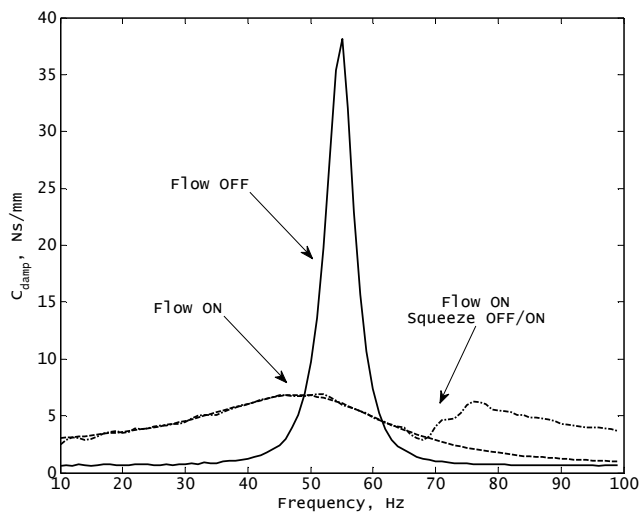


Fig. 33. Damping: simple control scheme

Finally, a simple control scheme was briefly analyzed in the present study. The tests involved exciting the mount with the sweep-sine displacement profile, powering the flow mode circuit, and switching the current on in the flow mode circuit above the resonance frequency. The effect is shown in Figs. 32 and 33. In a similar manner the effect can be controlled below the resonance frequency. The purpose of the test was to investigate the existing opportunities for controlling the MR mount performance characteristics.

## 5. SUMMARY

The purpose of the modeling study was to present a lumped parameter model of a mixed mode MR mount as well as to examine the opportunities for adapting the dynamic characteristics of the mount operating at one fundamental operation mode (flow or squeeze) or a combination of two modes (flow and squeeze). In addition to the MR effect that was introduced into the analysis by means of the Bingham plastic model the presented models capture the effects of rubber stiffness and damping, fluid chamber

compliance and the fluid inertia. The effects of cavitation in fluid chambers were not examined in the study. When energized, both modes result in distinct performance characteristics. The effect of increasing the magnetic field in the annulus contribute to higher damping/stiffness (and amplitudes of the peak at the resonance), whereas the squeeze mode shows as a rather uniformly distributed superposition on the flow mode characteristics. With the squeeze mode the best effect can be achieved with small gaps between the core and the squeezing plate and small amplitude displacements. The squeeze mode effect is additive. Briefly, the results indicate the mixed mode potential for varying the stiffness and the damping of the mount at any frequency region of interest. Shortly, the squeeze mode offers interesting engineering benefits; however, the device itself presents serious manufacturing challenges due to the low displacement amplitudes needed for achieving an optimum performance of the mount. Also, squeeze-mode fluid characterization study would need to be undertaken for further understanding of the material's rheology when operating in that mode and a suitable control scheme developed as well.

## REFERENCES

1. BWI Group, <http://www.bwigroup.com>
2. FEMM, <http://www.femm.info/wiki/HomePage>
3. Lord Corp., <http://www.lord.com>
4. Adiguna H., Tiwari M., Singh R., Tseng H., Hrovat D. (2003), Transient response of a hydraulic engine mount, *J Sound and Vib*, Vol. 268, 217–248.
5. Alexandridis A. A. (2007), The MagneRide System, *In Proceedings of US Vehicle Dynamics Expo*, Novi, Michigan.
6. Baudendistel T.A., Tewani S.G., Shores J.M., Long M.W., Longhouse R.E., Namuduri C.S., Alexandridis A.A. (2003), Hydraulic mount with magnetorheological fluid, US Patent No. 6,622,995 B2.
7. Baudendistel T.A., Tewani S.G., Long M.W., Dingle J. W. (2002), Hybrid hydraulic mount with magnetorheological fluid chamber, US Patent No. 6,414,761 B1.
8. Bolter, R., Janocha H. (1998), Performance of long-stroke and low-stroke MR fluid dampers, *In Proceedings of the SPIE Conference of the International Society of Optical Engineers* (Ed. L. P. Davis), Washington, Vol. 3327, 303–313, Washington.
9. Brigley M., Choi Y.-T., Wereley N., Choi S. B. (2007), Magnetorheological isolators using multiple fluid modes, *J of Int Mater Sys and Struct*, Vol. 12, No 18, 1143–1148.
10. Carlson D. J., Chrzan M, J. (1994), Magnetorheological fluid dampers, US Patent No. 5277281.
11. Farjoud A., Cavey R., Ahmadian M., Craft M. (2009), Magneto-rheological fluid behavior in squeeze mode, *J Smart Mater and Struct*, Vol. 18, 095001.
12. Farjoud A., Ahmadian M., Mahmoodi N., Zhang X., Craft M. (2011), Non-linear modeling and testing of magnetorheological fluids in low shear rate squeezing flows, *J Smart Mater and Struct*, Vol. 20, 085013.
13. Gavin H. P., Hanson R.D., Filisko F.E. (1996a), Electrorheological dampers, Part 1: Analysis and design, *ASME J of Appl Mech*; Vol. 63, No 9, 669–75.
14. Gavin H.P., Hanson R.D., Filisko F.E., (1996b), Electrorheological dampers, Part 2: Testing and modeling. *ASME J of Appl Mech*, Vol. 63, No 9, 676–82.

15. **Gopalswamy S., Linzell S. M., Jones G. L., Kruckemeyer W. C., Johnston G. L.** (1999), Magnetorheological fan clutch, US Patent No. 5,896,965.
16. **Goldasz J., Sapiński B.** (2011), Model of a squeeze-mode magnetorheological mount, *Solid State Phenomena*, Vol. 177, 116–124.
17. **He S., Singh R.** (2007), Transient response of hydraulic engine mount to a realistic excitation: improved non-linear models and validation, *SAE Technical Paper*, 2007-01-2365.
18. **Hong S. R., Choi S. B., Jung W. J., Jeong W. B.** (2002), Vibration isolation using squeeze-mode ER mounts, *J of Int Mater Sys and Struct*, Vol. 7, No 13, 421–424.
19. **Hopkins P. N., Fehring J. D., Lisenker I., Longhouse R. E., Kruckemeyer W. C., Oliver M. L., Robinson F. M., Alexandridis A. A.** (2001), Magnetorheological fluid damper, US Patent N. 6,311,810 B1.
20. **Jolly M. R., Bender J. W., Carlson J. D.** (1998), Properties and applications of magnetorheological fluids, *In Proceedings of the SPIE Conference of the International Society of Optical Engineers* (Ed. L. P. Davis), Washington, Vol. 3327, 262–275.
21. **Jolly M. R., Carlson J. D.** (1996), Controllable squeeze film damping using magnetorheological fluids, *In Proceedings of the 5th International Conference on New Actuators*, Bremen, 333–336.
22. **Kim G., Singh R.** (1993), Nonlinear analysis of automotive hydraulic engine mount, *Trans of the ASME*, Vol. 115, 482–487.
23. **Kim K.-J., Lee Ch.-W., Koo J.-H.** (2008), Design and modeling of semi-active squeeze film dampers using magnetorheological fluids, *J Smart Mater and Struct*, Vol. 17, doi: 10.1088/0964–1726/17/3/035006.
24. **Kowalczyk K., Svaricek F., Bohn C., Karkosch H.** (2004), An overview of recent automotive applications in active vibration control, *In Proceedings of the RTO AVT Symposium on Habitability of Combat and Transport Vehicles*, Prague, RTO-MP-AVT-110.
25. **Kruckemeyer W. C., Taeyoung H., Nehl T. W., Foister R. T.** (2001), Magnetorheological piston assembly and damper, US Patent Application No. 2006/0260891 A1.
26. **Lee K.** (1997), Numerical modelling for the hydraulic performance prediction of automotive monotube dampers, *J Veh Sys Dyn*, Vol. 28, 25–39.
27. **Minh N. T.** (2009), A novel semi-active magnetorheological mount for vibration isolation, Ph.D. Dissertation.
28. **Oliver M. L., Kruckemeyer W. C., Jensen E. L., Smith R. G.** (2003), Magnetorheological steering damper, US Patent No. 6,637,558 B2.
29. **Phillips R. W.** (1969), Engineering applications of fluids with a variable yield stress, Ph. D. Dissertation.
30. **Singh R., Kim G., Ravindra P.** (1992), Linear analysis of automotive hydromechanical mount with emphasis on decoupler characteristics, *J Sound and Vib*, Vol. 158, No. 2, 219–243.
31. **Sproston J. L., Rigby S. G., Williams E. W., Stanway R.** (1994), A numerical simulation of electrorheological fluids in oscillatory compressive squeeze-flow, *J. Phys D: Appl Phys*, Vol. 2, No 27, 338–340.
32. **Stanway R., Simms N.D., Johnson A.R.** (2000), Modelling and control of a magnetorheological vibration isolator, *In Proceedings of the SPIE Conference of the International Society of Optical Engineers*, Newport Beach, Vol. 3989, 184–193.
33. **Tang X., Wang X. J., Li W. H.** (1998), Testing and modeling of an MR damper in the squeeze flow mode, *In Proceedings of the 6th International Conference on ER Fluids, MR Suspensions and Their Applications* (Ed. M. Nakano and K. Koyama), Singapore, 870–878.
34. **Williams E., Rigby S. G., Sproston J., Stanway R.** (1993), Electrorheological fluids applied to an automotive engine mount, *J Non-Newtonian Fluid Mech*, Vol. 47, 221–238.
35. **Zhang X., Zhang H., Ahmadian M., Guo K.** (2011), Study on squeeze-mode magnetorheological engine mount with robust H-infinite control, *SAE Technical Paper*, 2011-01-0757.

**Acknowledgements:** The study is completed under the AGH-UST's research program No 11.11.130.560 sponsored through statutory research funds.